Journal of Solid State Chemistry 184 (2011) 911–914

Contents lists available at ScienceDirect

Journal of Solid State Chemistry

journal homepage: www.elsevier.com/locate/jssc

Local structure in solid solutions of stabilised zirconia with actinide dioxides (UO_2, NpO_2)

Marcus Walter [a,*], Joseph Somers [a], Daniel Bouëxière [a], Jörg Rothe [b]

[a] European Commission, Joint Research Centre, Institute for Transuranium Elements, P.O. Box 2340, D-76125 Karlsruhe, Germany
[b] Karlsruher Institut für Technologie, Institut für Nukleare Entsorgung (INE), P.O. Box 3640, D-76021 Karlsruhe, Germany

ARTICLE INFO

Article history:
Received 12 October 2010
Received in revised form
3 February 2011
Accepted 11 February 2011
Available online 19 February 2011

Keywords:
Transmutation
Nuclear fuel
Zirconium
Uranium
Neptunium
EXAFS

ABSTRACT

The local structure of $(Zr,Lu,U)O_{2-x}$ and $(Zr,Y,Np)O_{2-x}$ solid solutions has been investigated by extended X-ray absorption fine structure (EXAFS). Samples were prepared by mixing reactive $(Zr,Lu)O_{2-x}$ and $(Zr,Y)O_{2-x}$ precursor materials with the actinide oxide powders, respectively. Sintering at 1600 °C in Ar/H_2 yields a fluorite structure with U(IV) and Np(IV). As typical for stabilised zirconia the metal–oxygen and metal–metal distances are characteristic for the different metal ions. The bond lengths increase with actinide concentration, whereas highest adaptation to the bulk stabilised zirconia structure was observed for U–O and Np–O bonds. The Zr–O bond shows only a slight increase from 2.14 Å at 6 mol% actinide to 2.18 Å at infinite dilution in UO_2 and NpO_2. The short interatomic distance between Zr and the surrounding oxygen and metal atoms indicate a low relaxation of Zr with respect to the bulk structure, i.e. a strong Pauling behaviour.

1. Introduction

Cubic stabilised zirconia crystallises in a defect fluorite structure ($Fm\bar{3}m$), and forms solid solutions with actinide oxides. Due to its high thermal and radiation stability, stabilised zirconia is considered as a host matrix for plutonium and minor actinides (MA=Np, Am, Cm), either for their transmutation in dedicated reactor systems [1,2] or for conditioning in a radiation-resistant, durable form for final disposal [3,4]. In contrast, Zr and rare earth elements are important fission products and their progressive incorporation into the UO_2 lattice could alter the fuel properties during irradiation [5,6].

Information on the local atomic structure in such solid solutions assists in the understanding of mechanisms behind fuel or waste matrix properties and provides data for modelling their chemical and physical behaviour. Although X-ray diffraction reveals the lattice parameter of a solid solution, it is not suited to differentiate the local atomic structure of elements in the same crystallographic position. Such local structure information (bond lengths, coordination number, disorder) can be obtained from element specific methods such as extended X-ray absorption fine structure (EXAFS).

In principle, the bond length in an isovalent solid solution is limited by two cases, which reflect their ability to adapt to the bulk structure. Assuming that the atomic radii are approximately conserved (Pauling's concept), the individual bond length should be element specific and independent of the composition of the solid solution (i.e. no relaxation). In contrast, the virtual crystal approximation (VCA) could be valid and the bond lengths directly follow Vegard's law, similar to the lattice parameter (i.e. full relaxation) [7]. Early EXAFS investigations on both covalent and ionic systems [8] indicated that bond lengths follow an intermediate trend, i.e. they vary with the composition of the solid solution, but to a lower extend than expected by VCA. For example, such an intermediate behaviour is reported for the $(Th,U)O_2$ and $(Th,Pu)O_2$ solid solutions, where the relaxation is 32–35% for Th–O, but 47% and 54% for U–O and Pu–O, respectively [9,10]. In heterovalent solid solutions, like stabilised zirconia (YSZ), the bond lengths are also affected by the acceptance of vacancies and the associated reduction in the coordination number. The bond lengths in YSZ are element specific and nearly constant over a wide range of (Zr,Y) stoichiometries. [11,12]. EXAFS has been used to investigate the local structure of stabilised zirconia containing up to 20 mol% of actinides [13–16] and radiation effects in $Am_2Zr_2O_7$ [17,18]. Furthermore, EXAFS investigations covering a larger range in stoichiometry were performed on fluorite type solid solutions like $(U,Ce)O_2$ [19] and $(U,La)O_{2\pm x}$ [20].

The present work aims at the characterisation of the local structure of solid solutions containing stabilised zirconia and the actinide dioxides UO_2 and NpO_2 covering a wide stoichiometry

* Corresponding author. Present address: Verein für Kernverfahrenstechnik und Analytik e.V. (VKTA), P.O. Box 510119, D-01314 Dresden, Germany.
E-mail addresses: marcus.walter@vkta.de, 1052076@web.de (M. Walter).

0022-4596/$ - see front matter © 2011 Elsevier Inc. All rights reserved.
doi:10.1016/j.jssc.2011.02.014

range. Since $(Zr,Y)O_{2-x}$ is an envisaged matrix for nuclear application, $(Zr_{0.84}Y_{0.16})O_{1.92}$ and $(Zr_{0.5}Y_{0.5})_{1.75}$ were used to prepare $(Zr,Y,Np)O_{2-x}$ with two concentrations of oxygen vacancies. Unfortunately, the $(Zr,Y,U)O_{2-x}$ solid solution is not suited for conventional EXAFS investigations as the Y K (17,038 eV) and U L_3 (17,168 eV) edges are too close to derive structural information. Lutetium was selected to replace Y since it is invariably trivalent and does not form an ordered pyrochlore structure at $(Zr_{0.5}Lu_{0.5})O_{1.75}$.

2. Experimental

2.1. Sample preparation

$(Zr,Lu,U)O_{2-x}$ samples with Lu/Zr ratios of 0.2 and 1.0 were prepared by powder metallurgy using $(Zr,Lu)O_{2-x}$ precipitates calcined at 600 °C. The reactive stabilised zirconia precursor was mixed with U_3O_8 to obtain 6, 20, 50, 80, and 94 mol% U in $(Zr,Lu,U)O_{2-x}$. Pellets of the milled material were pressed and sintered at 1600 °C under Ar/H_2 atmosphere (24 h). After renewed milling, the material was pressed again and sintered under the same conditions. The $(Zr,Y,Np)O_{2-x}$ samples with 6, 20, 50, and 80 mol% Np were prepared in a similar manner starting from $(Zr,Y)O_{2-x}$ (Y/Zr=0.2 and 1.0) and NpO_2.

Powder X-ray diffraction patterns were obtained using a Bruker D8 diffractometer ($CuK\alpha_1$, Ge monochromator) equipped with a position sensitive detector (Vantec). Measurements were performed from 20 to 120° 2θ with incremental steps of 0.0085°. A single $Fm\bar{3}m$ phase was observed for all samples except $(Zr_{0.42}Lu_{0.08}U_{0.5})O_{1.96}$, where two cubic phases form. Attempts to prepare this compound by precipitation from a mixed Zr, Lu, U solution were also unsuccessful in obtaining a single phase.

2.2. EXAFS measurement

X-ray absorption spectra at the Zr, Y K-edge, and Lu, U and Np L_3-edge were recorded at the INE-Beamline [21] at the Ångströmquelle Karlsruhe, ANKA. The EXAFS oscillations were extracted according to standard procedures using WINXAS [22]. Spherical 8 Å clusters of atoms with the Cartesian coordinates of $(Zr,Lu,U)O_2$ and $(Zr,Y,Np)O_2$ were used for the calculation of the theoretical phase shifts, $\delta(k)$, and backscattering amplitude functions, $F(k)$, (FEFF8 [23]). The amplitude reduction factor was held constant at 1.0 for the EXAFS fits and the shift in threshold energy, ΔE_0, was varied as a global parameter. The EXAFS data were refined in R-space (1–4.5 Å) from the Fourier transformed k^3-weighted $\chi(k)$ data.

3. Results

The experimental EXAFS data for $(Zr_{0.67}Lu_{0.13}U_{0.20})O_{1.94}$ and $(Zr_{0.67}Y_{0.13}Np_{0.20})O_{1.94}$ are shown in Fig. 1 as an example. The k-range of the EXAFS data was limited by element absorption edges at next higher energies (e.g. Y K-edge EXAFS is limited by Np L_3-edge). The corresponding Fourier transforms (FT) reveals two peaks corresponding to approximately 8 oxygen and 12 metal (Zr+Lu+U or Zr+Y+Np) atoms, respectively. The experimental EXAFS data were fitted in R-space using fixed coordination numbers (N). The coordination number of the oxygen atoms was set to 8 for samples with Lu/Zr and Y/Zr=0.2. In case of the Lu/Zr and Y/Zr=1 samples N was set to values between 7 and 8, to account for the increase in oxygen vacancies with Y and Lu concentration.

Taking the different backscattering behaviour of Zr, Lu, U, and Np into consideration, the second FT peak was modelled with one or two metal backscatteres, depending on stoichiometry. For example,

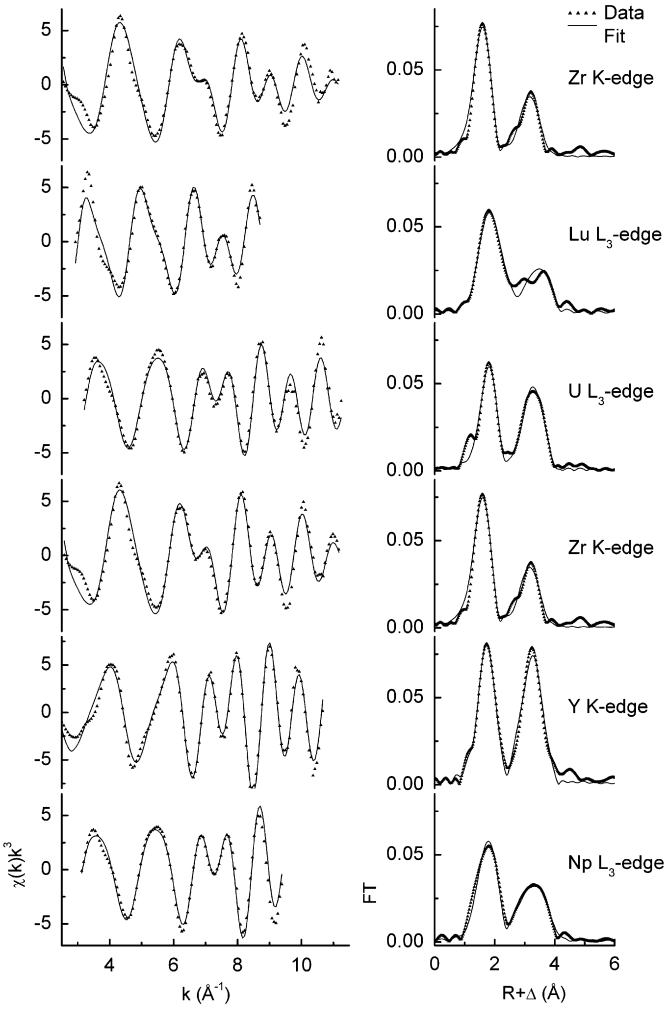

Fig. 1. k^3-weighted Zr, Y K-edge and Lu, U, Np L_3-edge EXAFS spectra of $(Zr_{0.67}Lu_{0.13}U_{0.20})O_{1.94}$ and $(Zr_{0.67}Y_{0.13}Np_{0.20})O_{1.94}$.

the second FT peak of samples with 94% actinide was modelled with 12 U atoms, as the Zr and Lu backscattering contribution is very low. To reduce the number of free parameters, Zr alone was chosen as backscatterer for Zr, Y and Lu (Lu/Zr=0.2 samples only) atoms in the second coordination shell. In addition, fits including all three metal atoms according to stoichiometry were tested, but the three metal–metal distances are too close to each other to derive meaningful structural parameters.

The Debye–Waller factor σ^2 for the two metal shells was correlated during the fit to minimise the strong correlation of the N, σ^2, and the backscattering amplitude of the different metal–metal paths. Because of the same reason an indepented refinement of metal coordination numbers and σ^2 was not performed and the obtained σ^2 values will not be discussed in the present paper.

A more distant coordination shell of 24 oxygen atoms at 4.3–4.5 Å ($R+\Delta$) had to be considered only for samples with high actinide content, as this coordination shell is strongly disordered in stabilised zirconia. The complete set of structural parameters is provided as Supplemental Data.

The derived metal–oxygen (M–O) bond distances are summarised in Figs. 2 and 3 for the $(Zr,Lu)O_{2-x}$–UO_2 and $(Zr,Y)O_{2-x}$–NpO_2 solid solutions, respectively. As is typical for stabilised zirconia compounds, the M–O lengths are element specific. The bond lengths in $(Zr_{0.79}Lu_{0.15}U_{0.06})O_{1.92}$ and $(Zr_{0.79}Y_{0.15}Np_{0.06})O_{1.92}$ are Zr–O 2.14 Å, Lu–O 2.27 Å, Np–O 2.27 Å, U–O 2.28 Å, and Y–O 2.31 Å. With increasing actinide content (i.e. lattice parameter)

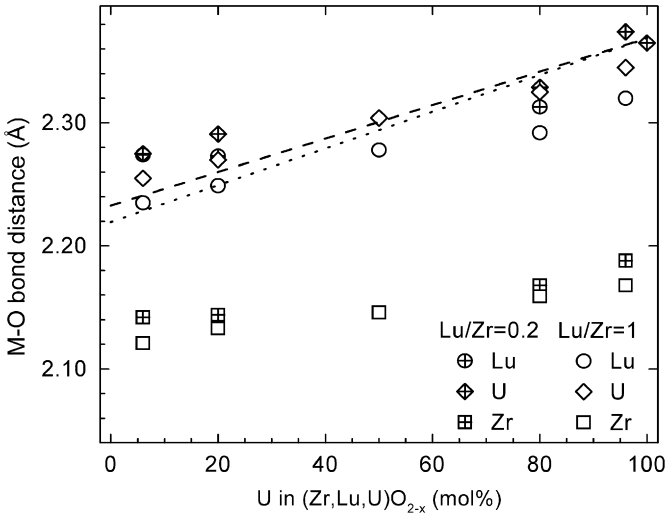

Fig. 2. Metal–oxygen bond distances in $(Zr,Lu,U)O_{2-x}$. The dotted (Lu/Zr=0.2) and dashed (Lu/Zr=1) lines correspond to the average M–O distance derived from the lattice parameter using Vegard's law.

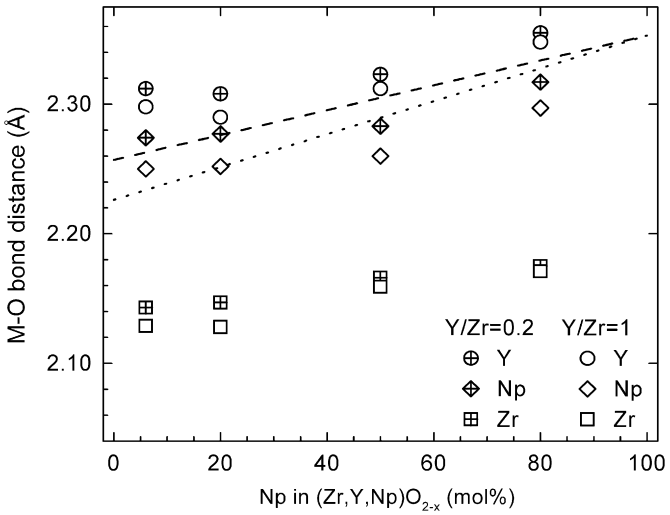

Fig. 3. Metal–oxygen bond distances in $(Zr,Y,Np)O_{2-x}$. The dotted (Y/Zr=0.2) and dashed (Y/Zr=1) lines correspond to the average M–O distance derived from the lattice parameter using Vegard's law.

the bond lengths increase. The bond lengths in the solid solutions with Lu/Zr=Y/Zr=1 are always slightly shorter than those with Lu/Zr=Y/Zr=0.2. Altough the difference is close to the error in determing interatomic distances by EXAFS (ΔR=0.01–0.02 Å), this effect is attributed to the lower coordination number for the larger concentration of oxygen vacancies caused by the trivalent Lu and Y atoms at Lu/Zr=Y/Zr=1.

The interatomic distances between the metal atoms in solid solutions can be distinguished due to the different backscattering behaviour of the metal atoms surrounding the selected central atom. As the backscattering phase shift and amplitude changes with increasing Z, structural information can be derived once ΔZ is sufficiently large, as in the case of Zr and Np. In contrast, atoms with similar Z (e.g. Zr and Y) cannot be distinguished as neighbouring atoms. However, the Zr–Y distance can be derived from the Y-edge when Zr is the dominating metal atom [14]. Fig. 4 shows the determined Zr–Zr/Y, Zr–Np, and Y–Np distances for the $(Zr,Y,Np)O_{2-x}$ solid solutions. The distance between the different metal atoms reflects the trend observed for the metal–oxygen bond lengths. The shortest distance is observed for the Zr–Zr/Y

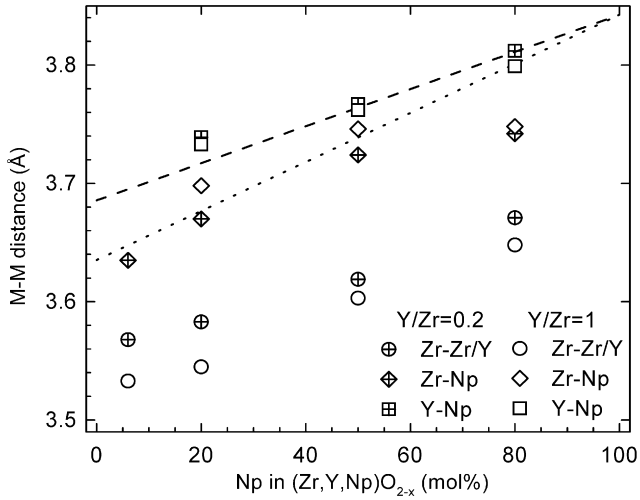

Fig. 4. Metal–metal interatomic distances in $(Zr,Y,Np)O_{2-x}$. The dotted (Y/Zr=0.2) and dashed (Y/Zr=1) lines correspond to the average M–M distance derived from the lattice parameter using Vegard's law.

atoms, whereas the larger metal atoms Y and Np also have the highest interatomic distance. Intermediate distances are observed for Zr–Np. A similar behaviour is observed for the other $(Zr,Y,Np)O_{2-x}$ and $(Zr,Lu,U)O_{2-x}$ solid solutions. Similar to the M–O bond lengths, the M–M distance increases with increasing Np content, i.e. lattice parameter. The Zr–Zr distance is significantly shorter for Y/Zr=1 than for Y/Zr=0.2 samples, which is in agreement with the shorter Zr–O bond length due to the oxygen vacancies (i.e. coordination number). This is not observed for the Y–Np distance and a slight increase of the Zr–Np distance is found for the higher Y/Zr ratio samples. Based on the different behaviour of the M–M distances in $(Zr,Y,Np)O_{2-x}$, some local ordering of the metal polyhedra can be assumed with increasing oxygen vacancy concentration. A close arrangement of irregular Zr–O polyhedra can be expected from the monoclinic ZrO_2 structure [24] and other EXAFS measurements on zirconia systems [14,18,25]. This might be hindered in case of the generally more regular Y and Np polyhedra as both Y_2O_3 and NpO_2 crystallise in cubic structures [26]. The M–M distances in $(Zr,Lu,U)O_{2-x}$ show a similar increasing trend with the U content. However, a detailed comparison of the Lu/Zr=0.2 and Lu/Zr=1 solid solutions is difficult due to the intermediate backscattering shift and amplitude of Lu.

4. Discussion and conclusion

On the zirconia rich side (6 mol% An) of the investigated solid solutions with Y/Zr=Lu/Zr=0.2, the determined An–O bond lengths are almost identical: U(IV)–O (2.28 Å), Np(IV)–O (2.27 Å), and Am(IV)–O (2.27 Å) [14]. According to the VCA approach a mean bond length of 2.23 Å is expected for this stoichiometry. Compared to the An–O bond length in the pure actinide dioxides (U–O 2.37 Å, Np–O 2.35 Å, and Am–O 2.33 Å [27]) the relaxation [7] of the measured An–O bond lengths in stabilised zirconia is about 60–70%. As U, Np, and Am have a comparable local structure in the zirconia host structure, a similar behaviour can be expected for the incorporation of Pu(IV) in stabilised zirconia. The Pu(IV)–O bond length should be approximately 2.27 Å, similar to Np(IV)–O and Am(IV)–O. A detailed discussion of the stabilisation mechanisms of actinides in a stabilised zirconia matrix is given in Refs. [13–16].

With increasing actinide content, the bond lengths determined by EXAFS increase, but to a different extent than the lattice parameter. A linear extrapolation of the measured Zr–O, Y–O,

and Lu–O bond distances to infinite dilution in pure UO_2 and NpO_2 results in Zr–O 2.18 Å, Y–O 2.36 Å, and Lu–O 2.33 Å. The same Zr–O bond length is then determined for its dilution in UO_2 and NpO_2, independent of the Lu/Zr and Y/Zr ratio. These values are quite close to bond lengths calculated using the bond valence method for 8-fold coordination of these elements in their formal valence [28]: Zr(IV)–O 2.19 Å, Y(III)–O 2.38 Å, and Lu(III)–O 2.33 Å or the bond lengths calculated by the ionic radii: Zr(IV)–O 2.22 Å, Y(III)–O 2.40 Å, and Lu(III)–O 2.36 Å [29]. Whereas the Y–O and Lu–O bond lengths are similar to those for such UO_2 (2.37 Å) and NpO_2 (2.35 Å) host structures, the determined Zr–O bond length indicates a substantial misfit between the Zr local and the UO_2 host structure. This observation may have a direct impact on nuclear fuel behaviour during irradiation. Zirconium is one of the important uranium fission products and it is found both dissolved in the UO_2 lattice and as a separate perovskite-type phase $(Ba,Sr,Cs)(U,Pu,Zr,Mo)O_3$ [5]. Zirconium solubility in pure UO_2 at reactor operation temperatures is quite low, but can be enhanced by the addition of rare earth elements like La, Nd, Ce [5,30]. The difference in the ionic radii of Zr and U and their different dioxide structures have been suggested as the reason for the low Zr solubility in UO_2 [31]. However, the present EXAFS data provide spectroscopic evidence that Zr is not able to relax its Zr–O bond beyond the limit posed by its ionic radius. This relaxation inability is the structural reason for the low solubility of Zr in UO_2 and explains why segregation of Zr and formation of a separate phase in spent fuel is possible. In contrast, U and Np can readily relax their bonds towards oxygen, and can easily be incorporated in the stabilised zirconia matrix host matrix.

Acknowledgment

We would like to acknowledge the assistance of C. Boshoven, S. Gardeur, M. Holzhäuser and P. Lajarge in the preparation of samples, and thank the Ångströmquelle Karlsruhe, ANKA, for providing beamtime for the EXAFS measurements.

Appendix A. Supplementary material

Supplementary data associated with this article can be found in the online version at doi:10.1016/j.jssc.2011.02.014

References

[1] A. Fernández, D. Haas, R.J.M. Konings, J. Somers, J. Am. Ceram. Soc. 85 (2002) 694–696.
[2] Y. Croixmarie, E. Abonneau, A. Fernández, R.J.M. Konings, F. Desmoulière, L. Donnet, J. Nucl. Mater. 320 (2003) 11–17.
[3] W.L. Gong, W. Lutze, R.C. Ewing, J. Nucl. Mater. 277 (2000) 239–249.
[4] G.R. Lumpkin, Elements 2 (2006) 365–372.
[5] H. Kleykamp, J. Nucl. Mater. 131 (1985) 221–246.
[6] T. Fujino, C. Miyake, in: A.J. Freeman, C. Keller (Eds.), Handbook on the Physics and Chemistry of the Actinides, Elsevier, Amsterdam, 1991, pp. 155–240.
[7] J.L. Martins, A. Zunger, Phys. Rev. B 30 (1984) 6217–6220.
[8] J.B. Boyce, J.C. Mikkelsen Jr., Phys. Rev. B 31 (1985) 6903–6905.
[9] J. Purans, G. Heisbourg, N. Dacheux, Ph. Moisy, S. Hubert, Phys. Scr. T115 (2005) 925–927.
[10] S. Hubert, J. Purans, G. Heisbourg, P. Moisy, N. Dacheux, Inorg. Chem. 45 (2006) 3887–3894.
[11] C.R.A. Catlow, A.V. Chadwick, G.N. Greaves, L.M. Moroney, J. Am. Ceram. Soc. 69 (1986) 272–277.
[12] D. Komyoji, A. Yoshiasa, T. Moriga, S. Emura, F. Kanamaru, K. Koto, Solid State Ionics 50 (1992) 291–301.
[13] P. Villella, S.D. Conradson, F.J. Espinosa-Faller, S.R. Foltyn, K.E. Sickafus, J.A. Valdez, Phys. Rev. B 64 (2001) 104101.
[14] M. Walter, C. Nästren, J. Somers, R. Jardin, M.A. Denecke, B. Brendebach, J. Solid State Chem. 180 (2007) 3130–3135.
[15] K. Holliday, T. Hartmann, F. Poineau, J.R. Kennedy, K. Czerwinski, J. Nucl. Mater. 393 (2009) 224–229.
[16] M. Walter, J. Somers, D. Bouëxière, P. Gaczynski, B. Brendebach, J. Solid State Chem. 182 (2009) 3305–3311.
[17] P.M. Martin, R.C. Belin, P.J. Valenza, A.C. Scheinost, J. Nucl. Mater. 385 (2009) 126–130.
[18] R.C. Belin, P.M. Martin, P.J. Valenza, A.C. Scheinost, Inorg. Chem. 48 (2009) 5376–5381.
[19] P. Martin, M. Ripert, T. Petit, T. Reich, C. Hennig, F. D'Acapito, J.L. Hazemann, O. Proux, J. Nucl. Mater. 312 (2003) 103–110.
[20] R.M. Rojas, M.P. Herrero, C. Bridges, A.V. Chadwick, C.R.A. Catlow, S.M. Tomlinson, J. Less-Common Met. 149 (1989) 115–120.
[21] J. Rothe, M.A. Denecke, K. Dardenne, T. Fanghänel, Radiochim. Acta 94 (2006) 691–696.
[22] T. Ressler, J. Synchrotron Rad. 5 (1998) 118–122.
[23] A.L. Ankudinov, B. Ravel, J.J. Rehr, S.D. Conradson, Phys. Rev. B 58 (1998) 7565–7576.
[24] D. Smith, H.W. Newkirk, Acta Crystallogr. 18 (1965) 983–991.
[25] P. Li, I.-W. Chen, J.E. Penner-Hahn, Phys. Rev. B 48 (1993) 10074–10081.
[26] R.G. Haire, L. Eyring, in: K.A. Gschneidner Jr., L. Eyring, G.R. Choppin, G.H. Lander (Eds.), Handbook on the Physics and Chemistry of Rare Earths, vol. 18, Lanthanides/Actinides: Chemistry, North-Holland, Amsterdam, 1994, pp. 413–505.
[27] D. Taylor, Br. Ceram. Trans. J. 83 (1984) 32–37.
[28] I.D. Brown, The Chemical Bond in Inorganic Chemistry, Oxford, New York, 2002 〈http://www.ccp14.ac.uk/ccp/web-mirrors/i_d_brown/bond_valence_param〉.
[29] R.D. Shannon, Acta Crystallogr. A 32 (1976) 751–767.
[30] F. Schleifer, A. Naoumidis, H. Nickel, J. Nucl. Mater. 101 (1981) 150–161.
[31] N.K. Kulkarni, K. Krishnan, U.M. Kasar, S.K. Rakshit, S.K. Sali, S.K. Aggarwal, J. Nucl. Mater. 384 (2009) 81–86.